



**HAL**  
open science

## **Simultaneous doping of Zn and Sb in SnO<sub>2</sub> ceramics: Enhancement of electrical conductivity.**

Iyad Saadeddin, Hikmat S. Hilal, Brigitte Pecquenard, J. Marcus, A. Mansouri, Christine Labrugère, M. A. Subramanian, Guy Campet

### ► **To cite this version:**

Iyad Saadeddin, Hikmat S. Hilal, Brigitte Pecquenard, J. Marcus, A. Mansouri, et al.. Simultaneous doping of Zn and Sb in SnO<sub>2</sub> ceramics: Enhancement of electrical conductivity.. Solid State Sciences, 2006, 8 (1), pp.7-13. 10.1016/j.solidstatesciences.2005.09.002 . hal-00018449

**HAL Id: hal-00018449**

**<https://hal.science/hal-00018449>**

Submitted on 9 Apr 2021

**HAL** is a multi-disciplinary open access archive for the deposit and dissemination of scientific research documents, whether they are published or not. The documents may come from teaching and research institutions in France or abroad, or from public or private research centers.

L'archive ouverte pluridisciplinaire **HAL**, est destinée au dépôt et à la diffusion de documents scientifiques de niveau recherche, publiés ou non, émanant des établissements d'enseignement et de recherche français ou étrangers, des laboratoires publics ou privés.

# Simultaneous doping of Zn and Sb in SnO<sub>2</sub> ceramics: Enhancement of electrical conductivity

I. Saadeddin<sup>a,\*</sup>, H.S. Hilal<sup>b</sup>, B. Pecquenard<sup>a</sup>, J. Marcus<sup>c</sup>, A. Mansouri<sup>d</sup>, C. Labrugere<sup>a</sup>,  
M.A. Subramanian<sup>e</sup>, G. Campet<sup>a,\*</sup>

<sup>a</sup> Institut de Chimie de la Matière Condensée de Bordeaux (CNRS-UPR9048), Université Bordeaux I, 87, Avenue de Dr. Albert Schweitzer, 33608 Pessac, France

<sup>b</sup> Department of Chemistry, An-Najah National University, PO Box 7, Nablus, Palestine

<sup>c</sup> Laboratoire d'Etudes des Propriétés Electroniques des Solides (CNRS-UPR11), 25, Avenue des Martyrs, 38000 Grenoble, France

<sup>d</sup> Institut Européen des Membranes (IEM), Université Montpellier II, Place Eugène Bataillon, 34095 Montpellier, France

<sup>e</sup> DuPont Central Research & Development, Experimental Station, Wilmington, DE 19880-0328, USA

---

## Abstract

SnO<sub>2</sub>-based ceramics doped with Sb and/or Zn, have been prepared by solid state reaction at 1300 °C. The effect of dopants on electronic properties and sintering behavior has been studied. While undoped SnO<sub>2</sub> pellets displayed very low electrical conductivities and lower densities, the Sb-doped ceramics showed higher electrical conductivity, with almost no densification and a significant antimony loss. On the contrary, a high densification and low conductivity are obtained for Zn-doped ceramics. Therefore, it is worthwhile to investigate SnO<sub>2</sub> ceramics co-doped with Sb and Zn (SnO<sub>2</sub>:Sb:Zn) to combine the advantages of both dopants. X-ray photoelectron spectroscopy (XPS) analysis confirmed that Sb<sup>5+</sup> is mainly substituted at the Sn<sup>4+</sup> site for Sb-doped ceramics and is in agreement with Hall-measurements. In the case of SnO<sub>2</sub> samples co-doped with Sb and Zn, XPS and Hall data confirmed the presence of both Sb<sup>5+</sup> and Sb<sup>3+</sup>. The SnO<sub>2</sub>:Sb:Zn system exhibited enhanced electrical conductivity and high densities. In addition, the presence of Zn prevented the Sb evaporation during sintering.

*Keywords* Tin dioxide; Doped ceramics; Electrical conductivity; Densification

---

## 1. Introduction

Tin (IV) dioxide, SnO<sub>2</sub>, has only one stable phase, the so-called cassiterite (mineral form). It crystallizes in the tetragonal rutile structure with space group  $P4_2/mnm$ , with lattice parameters  $a = b = 4.738 \text{ \AA}$  and  $c = 3.187 \text{ \AA}$  [1]. Tin dioxide is used in different technological areas, such as optoelectronic devices, gas-sensors and lithium batteries [2–6]. Some properties can be drastically changed by the addition of adequate dopants. For instance, undoped stoichiometric SnO<sub>2</sub> is an insulator; whereas doping with F<sup>-</sup> or Sb<sup>5+</sup> leads to a degenerate semiconductor with metal-like conductivity [7–9]. Moreover,

the high band-energy gap of SnO<sub>2</sub> ( $\sim 3.6 \text{ eV}$ ) is even more increased by such doping due to Moss–Brustein effect [10–12]. Metal-type conductivity together with a large band-energy gap, doped SnO<sub>2</sub> ceramic is specially attractive for manufacturing highly-conductive transparent thin film electrodes. Various techniques, such as sol–gel [13], chemical vapor deposition [14], spray pyrolysis [15,16], pulsed laser deposition [17] and sputtering [18] have all been experimented to prepare such thin film electrodes. In order to prepare large scale thin films with high deposition rates, the sputtering technique needs highly dense and conductive ceramic-based targets. Unfortunately, the use of SnO<sub>2</sub> ceramics is limited by the low densification of this oxide during sintering. Indeed, Leite et al. [19,20] and Varela et al. [21] reported no significant macroscopic shrinkage during sintering, even at up to 1300 °C. However, a meaningful shrinkage, associated with high densification, is possible by addition of cationic dopants with oxidation states lower than Sn<sup>4+</sup>, such

---

\* Corresponding authors. Tel.: +33 (05) 40 00 62 97; fax: +33 (05) 40 00 27 61.

*E-mail addresses* saadedin@icmcb-bordeaux.cnrs.fr (I. Saadeddin), campet@icmcb-bordeaux.cnrs.fr (G. Campet).

as  $\text{Mn}^{2+}$ ,  $\text{Cu}^{2+}$ ,  $\text{Zn}^{2+}$  or  $\text{Co}^{3+}$  [22–24]. In this work  $\text{SnO}_2$  was doped with both  $\text{Zn}^{2+}$  and  $\text{Sb}^{5+}$  ions in order to obtain dense ceramics with high electrical conductivities. It is assumed that doping  $\text{SnO}_2$  with  $\text{Sb}^{5+}$  may introduce free electrons in the semiconductor conduction band, while doping with  $\text{Zn}^{2+}$  induces high densification [22–24]. It is also assumed that doping with  $\text{Zn}^{2+}$  (having  $4s^0$  electronic structure) will not have much effect on  $\text{SnO}_2$  conduction band (with  $s$ -character). Therefore, the electron mobility, and thereby the conductivity, should not be much affected.

The aim of this work is to give an insight on how the doping elements influence the density, the structure, and the electronic properties of the  $\text{SnO}_2$ -based ceramics. A set of complementary investigation methods has been used to characterize the ceramics. The chemical composition of ceramics has been determined using Electron Probe X-ray Microanalysis (EPMA) and Thermogravimetric analysis (TGA). Structural analysis has been evaluated by X-Ray Diffraction (XRD) and Scanning Electron Microscopy (SEM). Finally, the electronic properties have been evaluated by X-ray Photoelectron Spectroscopy (XPS), resistivity and Hall measurements.

## 2. Experimental

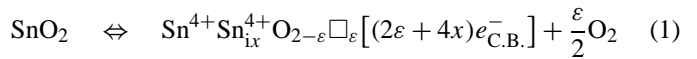
$\text{SnO}_2$  (99.9%, Aldrich),  $\text{Sb}_2\text{O}_3$  (> 99%, Prolabo) and  $\text{ZnO}$  (99.9%, Aldrich) powders, were used to prepare the  $\text{SnO}_2$  based ceramics. Appropriate amounts of the selected oxides were ball mixed for 30 min in an agate bowl containing agate balls and ethanol. The alcohol was then evaporated at  $110^\circ\text{C}$  for 6 hours. Afterwards, the powder was ground in an agate mortar, and pressed, in a mold, at 185 MPa, to form  $\sim 3$  mm thick cylindrical pellets, 13 mm in diameter. The pellets were finally sintered at  $1300^\circ\text{C}$  under air for 12 hours. The sintering temperature was chosen to minimize the oxygen departure [21]. Pellet dimensions were measured with a digital caliper vernier, and weighed using an analytical balance. These measurements were used to estimate the bulk densities of the pellets. For some samples, the bulk densities were also determined precisely from mercury displacement method using an AutoPore IV 9500 mercury porosimeter. The latter was also used to determine the pore size distribution. Scanning electron microscopy (SEM) was measured on a JEOL JSM-6360 microscope. To protect samples from charging by the electron beam, during observation, the samples were coated with a thin gold film. Thermo-gravimetric analysis (TGA) was recorded on a 2950 HR V 5.3 TGA apparatus. Annealing was done in the range  $25$ – $1300^\circ\text{C}$  under air at  $5^\circ\text{C min}^{-1}$  annealing rate. Pellet chemical compositions were determined by Electron Probe X-ray Microanalysis (EPMA) using a CAMECA SX100 spectrometer. XRD data were acquired on a Philips PW1820 vertical goniometer with in a Bragg Brentano geometry with  $\text{CuK}_\alpha$  radiation ( $\lambda = 1.5406 \text{ \AA}$ ). The XPS data were collected using a VG 220i-XL Escalab spectrometer with a non-monochromatized  $\text{AlK}_\alpha$  source ( $h\nu = 1486.6 \text{ eV}$ ) at 110 Watt and a 10 eV pass energy for high-resolution spectra. Energy calibration for XPS was done using Silver. Fresh samples were

fractured and quickly transferred to the ultra-high vacuum system. Resistivity was measured, as a function of temperature, from 4.2 K to room temperature, using computerized home-made four-probe equipment. Conduction-band majority carrier (electrons) concentrations were determined from Hall measurements in a magnetic field strength ranging from 0 to 3 T. Typical used ceramic dimensions were  $2 \times 2 \text{ mm}^2$  with thickness range 0.1–0.3 mm.

## 3. Results and discussion

### 3.1. $\text{SnO}_2$ ceramics

Consistent with literature [19–21], no significant macroscopic shrinkage was observed for undoped ceramics by sintering at  $1300^\circ\text{C}$ . The bulk density ( $4.12 \text{ g/cm}^3$ ), corresponds to 58% of the theoretical value ( $6.95 \text{ g/cm}^3$ ), as shown in Table 1. It should be noted that the n-type conductivity, normally observed in undoped  $\text{SnO}_2$ , is due to the co-existence of oxygen vacancies ( $\square$ ) and interstitial tin ( $\text{Sn}_i$ ), occurring simultaneously and producing shallow donor levels [11]. Therefore the n-type conduction in undoped  $\text{SnO}_2$  can be reasonably depicted with the following formula:



where  $e^-$  represents the mobile electrons in the lattice. In this work, the ceramics, white in color, have a rather low electrical conductivity ( $\sim 10^{-4} \text{ S cm}^{-1}$ ). Such n-type conductivity low value means that  $\varepsilon$ , depicted in formula (1), is lower than  $10^{-2}$  [25]. Consequently, it can possibly be asserted that practically no oxygen departs from the  $\text{SnO}_2$  lattice at temperatures up to  $1300^\circ\text{C}$ , in agreement with literature [19]. This was confirmed by TGA analysis (Fig. 1(a)). Only small weight losses ( $\sim 0.4\%$ ) take place in the temperature range  $25$ – $500^\circ\text{C}$ . Such weight losses are due to adsorbed water removal and structural water removal from Sn–OH moieties present on the grain surface [26,27]. In the temperature range  $500$ – $1300^\circ\text{C}$ , no weight loss is observed.

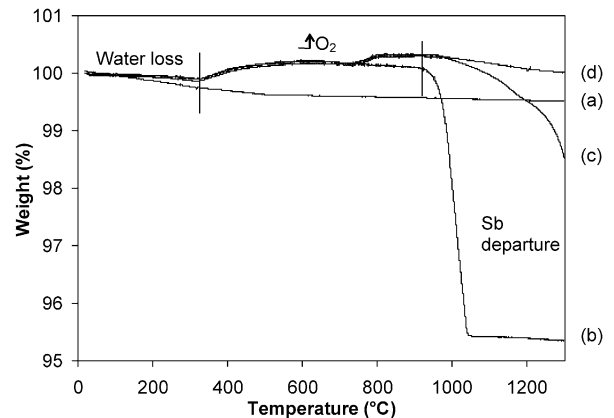


Fig. 1. TGA data for (a)  $\text{SnO}_2$ , (b)  $\text{SnO}_2\text{:Sb}_{0.06}$ , (c)  $\text{SnO}_2\text{:Sb}_{0.06}\text{:Zn}_{0.02}$ , and (d)  $\text{SnO}_2\text{:Sb}_{0.06}\text{:Zn}_{0.06}$ .

Table 1

Ceramic chemical composition, volumetric mass, and weight loss of  $\text{SnO}_2\text{:Sb}_x$  and  $\text{SnO}_2\text{:Sb}_{0.06}\text{:Zn}_y$  ceramics,  $0 \leq x \leq 0.10$  and  $0 \leq y \leq 0.14$ 

Entry number	Sample identification	Starting mixture	Ceramic final composition determined by EPMA	Bulk density ( $\text{g}/\text{cm}^3$ ) $\pm 0.05$	Weight loss <sup>a</sup> (%) $\pm 0.1$
1	$\text{SnO}_2$	$\text{SnO}_2$	$\text{SnO}_2$	4.12	0.4
2	$\text{SnO}_2\text{:Sb}_{0.02}$	$(\text{SnO}_2)_{0.98} + (\text{Sb}_2\text{O}_3)_{0.01}$	$\text{Sn}_{0.989}\text{Sb}_{0.011}\text{O}_2$	4.06	1.2
3	$\text{SnO}_2\text{:Sb}_{0.04}$	$(\text{SnO}_2)_{0.96} + (\text{Sb}_2\text{O}_3)_{0.02}$	$\text{Sn}_{0.987}\text{Sb}_{0.013}\text{O}_2$	4.02	3.0
4	$\text{SnO}_2\text{:Sb}_{0.06}$	$(\text{SnO}_2)_{0.94} + (\text{Sb}_2\text{O}_3)_{0.03}$	$\text{Sn}_{0.988}\text{Sb}_{0.012}\text{O}_2$	3.79	5.0
5	$\text{SnO}_2\text{:Sb}_{0.10}$	$(\text{SnO}_2)_{0.90} + (\text{Sb}_2\text{O}_3)_{0.05}$	$\text{Sn}_{0.987}\text{Sb}_{0.013}\text{O}_2$	3.47	8.9
6	$\text{SnO}_2\text{:Sb}_{0.06}\text{:Zn}_{0.02}$	$[(\text{SnO}_2)_{0.94} + (\text{Sb}_2\text{O}_3)_{0.03}]_{0.98} + (\text{ZnO})_{0.02}$	$\text{Sn}_{0.948}\text{Sb}_{0.035}\text{Zn}_{0.017}\text{O}_2$	4.51	1.2
7	$\text{SnO}_2\text{:Sb}_{0.06}\text{:Zn}_{0.06}$	$[(\text{SnO}_2)_{0.94} + (\text{Sb}_2\text{O}_3)_{0.03}]_{0.94} + (\text{ZnO})_{0.06}$	$\text{Sn}_{0.892}\text{Sb}_{0.053}\text{Zn}_{0.055}\text{O}_2$	6.42	~
8	$\text{SnO}_2\text{:Sb}_{0.06}\text{:Zn}_{0.10}$	$[(\text{SnO}_2)_{0.94} + (\text{Sb}_2\text{O}_3)_{0.03}]_{0.90} + (\text{ZnO})_{0.10}$	$\text{Sn}_{0.865}\text{Sb}_{0.053}\text{Zn}_{0.082}\text{O}_2$	6.24	~
9	$\text{SnO}_2\text{:Sb}_{0.06}\text{:Zn}_{0.14}$	$[(\text{SnO}_2)_{0.94} + (\text{Sb}_2\text{O}_3)_{0.03}]_{0.86} + (\text{ZnO})_{0.14}$	$\text{Sn}_{0.810}\text{Sb}_{0.052}\text{Zn}_{0.137}\text{O}_2$	6.07	~

The reported bulk densities were deduced by measuring pellets dimensions and weights. *Samples identification is the same for all following figures and tables.*

<sup>a</sup> ~ indicates negligible weight loss.

### 3.2. $\text{SnO}_2\text{:Sb}$ ceramics

Doping  $\text{SnO}_2$  with different nominal amounts of Sb significantly lowers the ceramic resistivity (Fig. 2). Similar to undoped  $\text{SnO}_2$ , the effects of oxygen vacancies and interstitial tin, are negligible in  $\text{SnO}_2\text{:Sb}_x$  ceramics. Therefore, the resistivity lowering could result from carrier concentration increase, according to the following formulas

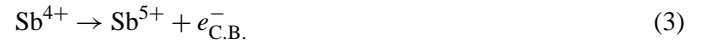


or



depending on whether Sb is being substitutional (formula (2a)) or interstitial (formula (2b)); where  $xe^-$  represents the number of free electrons in the conduction band per formula unit. According to formula (2b), the carrier concentration should be 5 times higher than the Sb content. However, it will be shown later, by Hall measurements, that mobile electrons concentration is nearly equal to Sb concentration in the  $\text{SnO}_2\text{:Sb}_x$  samples. This means that formula (2b) should be excluded and only formula (2a) should be adopted. Moreover the substitution is

facilitated by  $\text{Sb}^{5+}$  ionic radius (0.62 Å) [28] which is slightly smaller than that of  $\text{Sn}^{4+}$  (0.71 Å) in octahedral environment. The energy of the  $\text{Sb}^{4+}:5s^1$ , is located at the immediate vicinity of the conduction band edge [29], leading to metal type conductivity resulting from:



EPMA results for final compositions after ceramic sintering, are shown in Table 1, together with nominal compositions. It has been found that whatever the nominal antimony amount is, the final antimony composition always reaches only 0.01 moles per formula unit. Consequently, the significant weight loss reported in Table 1 accounts not only for water loss, but also for antimony oxide departure at high temperature during ceramic sintering. Moreover, the bulk density values of the Sb-doped ceramics are lower than their undoped counterparts (Table 1), presumably due to antimony departure during sintering. The weight loss (or gain) is more precisely observable from TGA data. As shown in Fig. 1(b), weight loss up to ( $\sim 0.1\%$ ) at  $340^\circ\text{C}$  can be assigned to the release of water departure (both adsorbed water and water resulting from surface hydroxyl group condensations). This parallels water loss that occurred in undoped  $\text{SnO}_2$ . The weight gain observed at temperatures above  $\sim 340^\circ\text{C}$  is probably due to the oxidation of  $\text{Sb}^{3+}$  to  $\text{Sb}^{5+}$  which in turn enters the structure to substitute  $\text{Sn}^{4+}$  according to formula (2), as confirmed hereafter by XPS analysis. Finally, the weight loss that occurs above  $\sim 940^\circ\text{C}$  is due to unreacted antimony oxide ( $\text{Sb}_2\text{O}_3$ ) departure. Fig. 3(a) represents the XPS data showing Sb (4d) spectra for  $\text{SnO}_2\text{:Sb}_{0.06}$  compound. A pronounced maximum occurs at 35.0 eV corresponding to  $\text{Sb}^{5+}$  species [30]. This confirms that antimony presents in  $\text{SnO}_2\text{:Sb}_x$  samples mostly occurs in the  $\text{Sb}^{5+}$  state. By taking into account formula (2a) and EPMA results, (showing that 0.01 Sb are present in the ceramic, Table 1); the carrier concentration is estimated to be  $1.4 \times 10^{20} e^- \text{cm}^{-3}$ . From Hall measurements, carrier concentrations were found to be in the range 1.2 to  $1.6 \times 10^{20} e^- \text{cm}^{-3}$  (Table 2), confirming our initial hypothesis and  $\text{Sb}^{5+}$  presence in substitution. Consequently, it can be deduced that (i) Sb solubility within  $\text{SnO}_2$  lattice is limited to  $\sim 1\%$  in agreement with literature [16]; (ii) most of Sb introduced in the crystal lattice plays a role in the conduction mechanism, according to formula (2) implying that Sb sub-

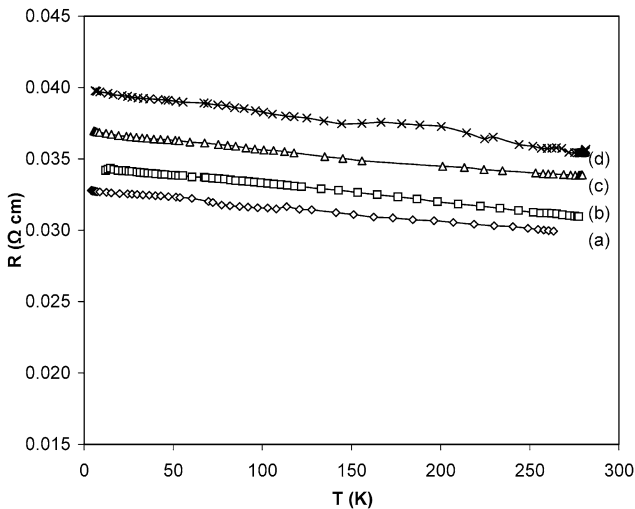


Fig. 2. Plots of resistivity versus temperature for  $\text{SnO}_2\text{:Sb}_x$  ceramics; (a)  $\text{SnO}_2\text{:Sb}_{0.02}$ , (b)  $\text{SnO}_2\text{:Sb}_{0.04}$ , (c)  $\text{SnO}_2\text{:Sb}_{0.06}$ , and (d)  $\text{SnO}_2\text{:Sb}_{0.10}$ .

Table 2  
Electrical measurements, conducted at room temperature, for  $\text{SnO}_2:\text{Sb}_x$  and  $\text{SnO}_2:\text{Sb}_{0.06}:\text{Zn}_y$  ceramics

Entry number	Sample identification <sup>a</sup>	Carrier concentration ( $10^{20} \text{ e}^- \text{ cm}^{-3}$ ) $\pm 2\%$	Resistivity ( $10^{-2} \Omega \text{ cm}$ ) $\pm 5\%$	Carrier mobility ( $\text{cm}^2 \text{ V}^{-1} \text{ s}^{-1}$ ) $\pm 5\%$
1	$\text{SnO}_2:\text{Sb}_{0.02}$	1.22	3.00	1.71
2	$\text{SnO}_2:\text{Sb}_{0.04}$	1.60	3.09	1.26
3	$\text{SnO}_2:\text{Sb}_{0.06}$	1.25	3.38	1.48
4	$\text{SnO}_2:\text{Sb}_{0.06}:\text{Zn}_{0.06}$	1.15	1.28	4.26
5	$\text{SnO}_2:\text{Sb}_{0.06}:\text{Zn}_{0.10}$	0.97	1.37	4.69
6	$\text{SnO}_2:\text{Sb}_{0.06}:\text{Zn}_{0.14}$	0.95	1.40	4.71

<sup>a</sup> See Table 1.

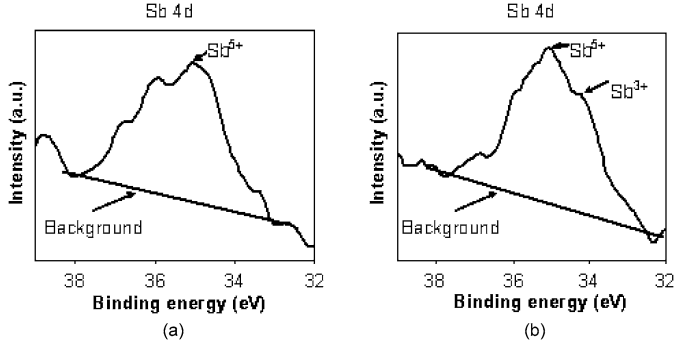


Fig. 3. Sb 4d XPS normalized spectra for (a)  $\text{SnO}_2:\text{Sb}_{0.06}$  ceramic, (b)  $\text{SnO}_2:\text{Sb}_{0.06}:\text{Zn}_{0.06}$  ceramic. Similar observations were observed for other antimony and antimony-zinc doped ceramics.

stitutes  $\text{Sn}^{4+}$  in the lattice as  $\text{Sb}^{5+}$ . Taking into account the carrier concentration determined from Hall effect and the conductivity measurements, the carrier mobility ( $\mu$ ) is estimated to be  $\sim 1 \text{ cm}^2 \text{ V}^{-1} \text{ s}^{-1}$  (Table 2). This value is about ten times smaller than that occurring in dense thin films, for similar carrier concentration [31,32]. In this work, the mobility is limited by a textural effect. First of all, the intrinsic carrier mean free path must be negligible compared with the crystallite size. Otherwise, the carrier-scattering effect occurring at the crystallite interfaces will cause a carrier mobility lowering [25]. From X-ray diffractogram (Fig. 4), the crystallite mean size is estimated to be  $\sim 60 \text{ nm}$  by using the Scherrer formula. This value is more than 100 times higher than the electron mean free path. Indeed, the electron mean free path,  $l$ , can be roughly estimated from the classical relation:

$$l = \mu \tau \quad (4)$$

where  $v = (3kT/m^*)^{1/2}$  is the electron velocity,  $m^*$  is the electron effective mass and  $\tau = \mu m^*/e^2$  is the relaxation time. By assuming an intrinsic mobility  $\mu \sim 10 \text{ cm}^2 \text{ V}^{-1} \text{ s}^{-1}$ , and taking  $m^* \sim 0.19\text{--}0.33m_0$  [33], then  $l$  is  $\sim 0.29\text{--}0.38 \text{ nm}$ . Consequently, the electron mean free path may be neglected in comparison with the average crystallite size. Moreover, the effect of crystallite interfaces is weaker in heavily doped semiconductors, with  $n \geq 10^{20} \text{ cm}^{-3}$ , observed here, as a consequence of the narrower depletion layer width at the interface between two crystallites [34]. Consequently, the observed low carrier mobility,  $\mu \sim 1 \text{ cm}^2 \text{ V}^{-1} \text{ s}^{-1}$  (Table 2), cannot be justified using a straightforward carrier-scattering effect occurring

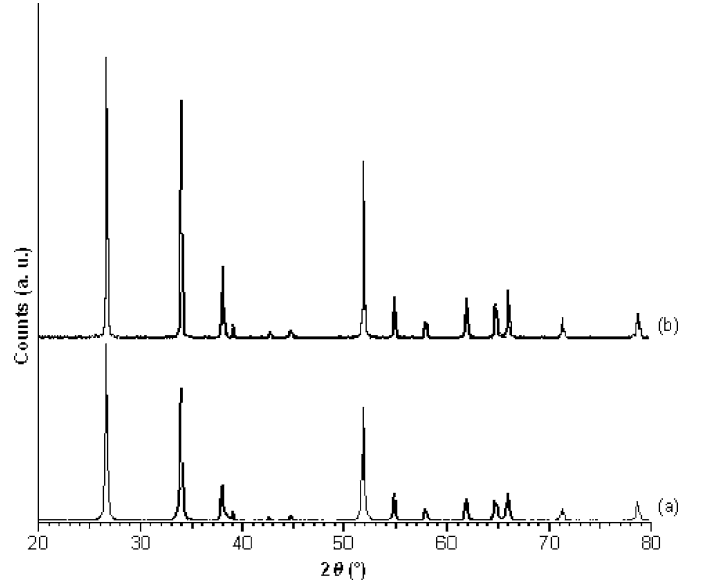


Fig. 4. XRD data for (a) undoped  $\text{SnO}_2$  and (b)  $\text{SnO}_2:\text{Sb}_{0.06}$  powders annealed at  $1300^\circ \text{C}$ . Same peak positions appear for  $\text{SnO}_2$ , no extra peaks is observed. The only difference comes from a slight decrease in line width for  $\text{SnO}_2:\text{Sb}_{0.06}$ .

at the crystallite interfaces. Moreover, one has to emphasize that the ceramic density should approach as much as possible the theoretical density. Indeed, an inefficient grain percolation and/or the presence of pores in the ceramics, will also cause a drop of the carrier mobility and, therefore, a drop of the conductivity [35]. Such textural aspects appears on the SEM micrographs (Fig. 5) showing that the  $\text{SnO}_2:\text{Sb}_x$  samples consist of agglomerated particles, with rather regular sizes of micrometer order. This induces the existence of macropores and, thereby, leads to the low density values reported in Table 1. The presence of macropores is also evidenced from porosity measurements using a mercury porosimeter, Fig. 6, showing the variation of the differential intrusion of mercury versus pore size for doped  $\text{SnO}_2:\text{Sb}_x$  samples. Moreover, Fig. 6 indicates that as the nominal antimony content increases, the average pore size slightly increases. Main data deduced from porosity measurements are collected in Table 3. This parallels the bulk density decrease with the nominal antimony content increase, attributed to the antimony departure. Consequently, the mobility values obtained here are lower than expected, presumably due to the porous texture of the ceramics.

Table 3  
Main data deduced from porosity measurements for SnO<sub>2</sub>:Sb<sub>x</sub> ceramics

Entry number	Sample identification <sup>a</sup>	Total pore volume (cm <sup>3</sup> /g)	Average pore diameter (μm)	Bulk density <sup>b</sup> (g/cm <sup>3</sup> )
1	SnO <sub>2</sub> :Sb <sub>0.04</sub>	0.079	0.887	4.25
2	SnO <sub>2</sub> :Sb <sub>0.06</sub>	0.102	0.941	3.805
3	SnO <sub>2</sub> :Sb <sub>0.10</sub>	0.105	1.342	3.443

<sup>a</sup> See Table 1.

<sup>b</sup> The deduced bulk density values are, as expected, close to those listed in Table 1.

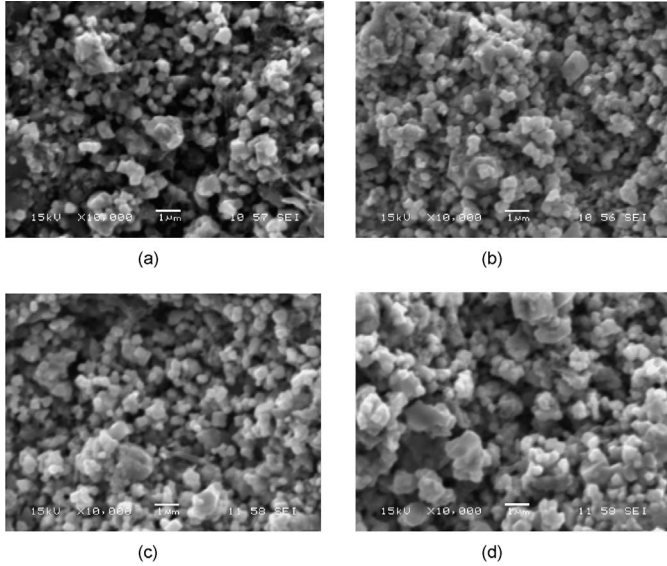


Fig. 5. SEM micrograph for SnO<sub>2</sub>:Sb<sub>x</sub> ceramics; (a) SnO<sub>2</sub>:Sb<sub>0.02</sub>, (b) SnO<sub>2</sub>:Sb<sub>0.04</sub>, (c) SnO<sub>2</sub>:Sb<sub>0.06</sub>, and (d) SnO<sub>2</sub>:Sb<sub>0.10</sub>.

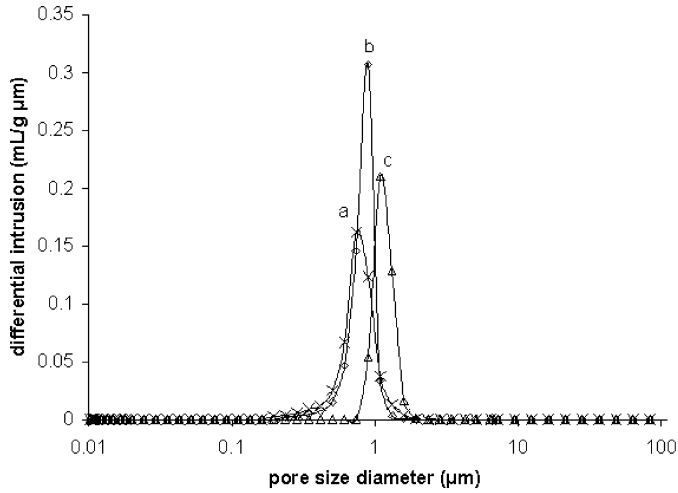


Fig. 6. Pore size diameter variation with Sb variation in SnO<sub>2</sub>:Sb<sub>x</sub> ceramics, (a) SnO<sub>2</sub>:Sb<sub>0.04</sub>, (b) SnO<sub>2</sub>:Sb<sub>0.06</sub>, and (c) SnO<sub>2</sub>:Sb<sub>0.10</sub>.

### 3.3. SnO<sub>2</sub>:Zn ceramics

According to literature [22–24], doping SnO<sub>2</sub> with substitutional cations, having lower oxidation states than Sn<sup>4+</sup>, strongly enhances the ceramic density. Therefore, as expected, the doping of SnO<sub>2</sub> with Zn<sup>2+</sup> greatly enhances the relative ceramic bulk density ( $\rho/\rho_0$ ), where  $\rho$  is the measured bulk density and

$\rho_0$  is the SnO<sub>2</sub> theoretical density. For example, when SnO<sub>2</sub> is doped with 0.06 at. of Zn, the relative bulk density increases up to 95%. It can be reasonably assumed that this event is correlated with the presence of Zn<sup>2+</sup> in substitutional positions, leading to the formation of uncharged oxygen vacancies according to:



Indeed, the presence of oxygen vacancies, as it occurs in formula (5), would promote mass transport at the grain boundary resulting in ceramics with higher densities. Let us quote that the presence of Zn<sup>2+</sup> (0.74 Å) [28] in interstitial position, leading to n-type conductivity according to:



can be reasonably neglected regarding the high value of the resistivity reported in Fig. 7.

### 3.4. SnO<sub>2</sub>:Sb:Zn ceramics

In order to combine the advantages of doping with both Sb<sup>5+</sup> and Zn<sup>2+</sup>, SnO<sub>2</sub>:Sb:Zn ceramics have been prepared. It noticeable from Table 1 (entries 6–9) that the sintered ceramics have an antimony concentration higher than the solubility limit (~ 0.01 at.) observed for the SnO<sub>2</sub>:Sb<sub>x</sub> ceramics. This implies that the ceramic shrinkage due to Zn doping prevents antimony departure, as observed in Table 1. Therefore, more Sb<sup>5+</sup> could eventually substitute Sn<sup>4+</sup> in the SnO<sub>2</sub>:Sb:Zn ceramic, leading to enhanced conductivity. The ceramics show higher electrical conductivity compared to the SnO<sub>2</sub>:Sb<sub>x</sub> system

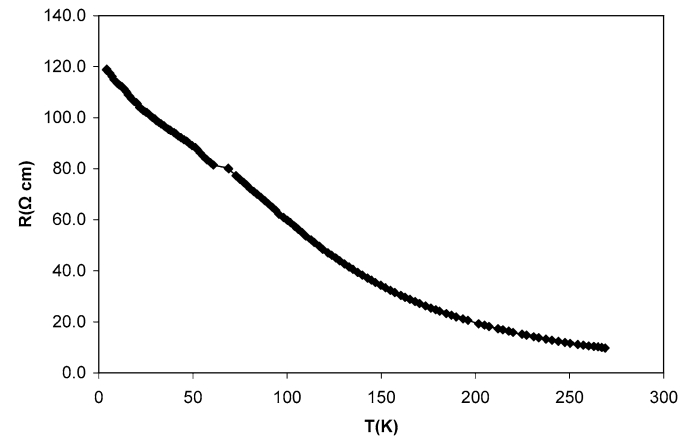


Fig. 7. A plot of resistivity versus temperature for SnO<sub>2</sub> doped with 0.06 at. of Zn.

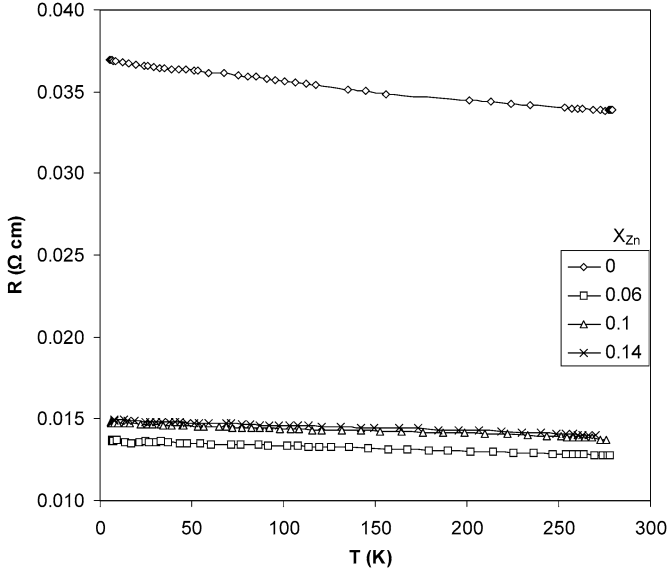


Fig. 8. Plots of resistivity versus temperature for different Zn atomic ratios ( $X_{Zn}$ ) in the  $\text{SnO}_2\text{:Sb}_{0.06}\text{:Zn}_y$  ceramics (see Table 1 legend).

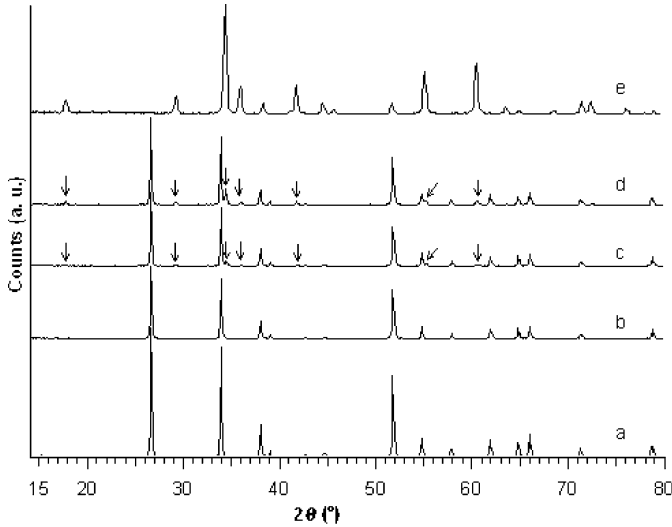


Fig. 9. XRD for (a)  $\text{SnO}_2\text{:Sb}_{0.06}$ , (b)  $\text{SnO}_2\text{:Sb}_{0.06}\text{:Zn}_{0.06}$ , (c)  $\text{SnO}_2\text{:Sb}_{0.06}\text{:Zn}_{0.10}$  (d)  $\text{SnO}_2\text{:Sb}_{0.06}\text{:Zn}_{0.14}$ , (e) inverse spinel  $\text{Zn}_2\text{SnO}_4$  phase. (↓) indicates peaks corresponding to the inverse spinel  $\text{Zn}_2\text{SnO}_4$  phase peaks.

(Fig. 8). The best conductivity ( $\sim 0.7 \times 10^2 \text{ S cm}^{-1}$  at 273 K), is reached for the ceramic doped with 0.06 atomic ratio of Zn. Most interestingly, the conductivity remains nearly stable over the whole temperature range. For higher Zn content, a resistivity increase has been noticed. This could be correlated with the formation of the insulating inverse spinel phase  $\text{Zn}_2\text{SnO}_4$  [36], as observed on the X-ray diffractogram (Fig. 9(c), (d)). Fig. 10 shows two steps: in the first step, the relative bulk density of the ceramic increases significantly as  $\text{Zn}^{2+}$  content increases from 0 to  $\sim 0.06$ . Then, in the second step, the bulk density slightly decreases with higher Zn values. This is probably due to inverse spinel phase formation. Therefore, the increase of the electrical conductivity can be reasonably explained by macroscopic carrier mobility enhancement, whereas grain percolation takes place due to mass transport at the grain boundary, as dis-

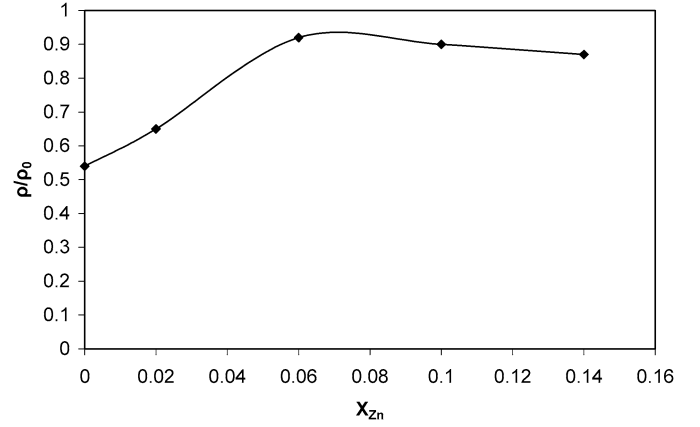


Fig. 10. Relative bulk density ( $\rho/\rho_0$ ) variation with  $X_{Zn}$  variation of  $\text{SnO}_2\text{:Sb}_{0.06}\text{:Zn}_y$  (see Table 1) ceramics.

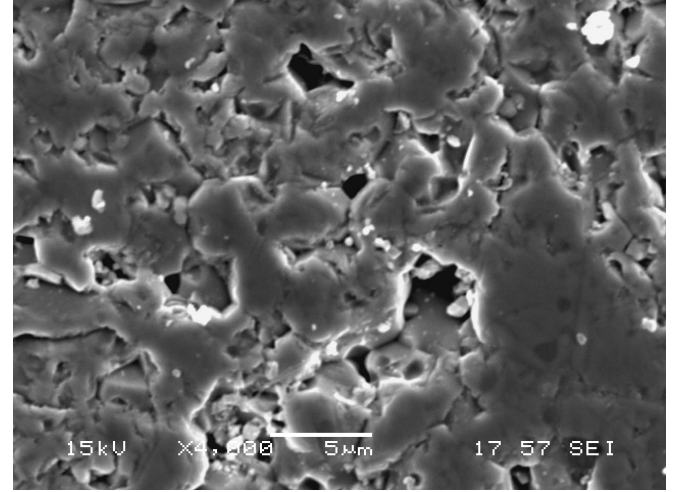
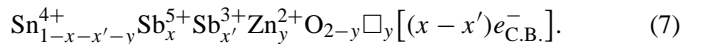


Fig. 11. SEM micrograph for  $\text{SnO}_2\text{:Sb}_{0.06}\text{:Zn}_{0.06}$  ceramic.

cussed above. Such grain percolation is evidenced on the SEM micrograph (Fig. 11) for the  $\text{SnO}_2\text{:Sb}_{0.06}\text{:Zn}_{0.06}$  ceramic. Moreover, Hall measurements reveal a significant enhancement in the carrier mobility, for the  $\text{SnO}_2\text{:Sb}_{0.06}\text{:Zn}_y$  ceramics, up to four times compared with  $\text{SnO}_2\text{:Sb}_x$  counterparts (Table 2). Such mobility enhancement is accompanied with a slight decrease in the carrier concentration,  $\sim 1 \times 10^{20} \text{ e}^{-}\text{cm}^{-3}$ . This result is a priori unexpected since the  $\text{SnO}_2\text{:Sb}_{0.06}\text{:Zn}_y$  ceramics have an antimony concentration higher than the solubility limit ( $\sim 0.01$  at.) observed for the  $\text{SnO}_2\text{:Sb}_x$  ceramics. In order to justify this ‘anomaly’, we should consider that the antimony in  $\text{SnO}_2\text{:Sb}_{0.06}\text{:Zn}_y$  sample is not purely  $\text{Sb}^{5+}$ , but  $\text{Sb}^{3+}$  and/or  $\text{Sb}^{4+}$  may also exist. In fact, we will show hereafter that only  $\text{Sb}^{5+}$  and  $\text{Sb}^{3+}$  are present in the n-type semiconductor according to:



First of all, XPS normalized Sb (4d) spectra for  $\text{SnO}_2\text{:Sb}_{0.06}\text{:Zn}_{0.06}$  ceramic (Fig. 3(b)) shows a recognized maximum at 35.0 eV (i.e.,  $\text{Sb}^{5+}$ ) and a new shoulder at around 34.2 eV confirming the existence of  $\text{Sb}^{3+}$  species [30]. The deduced  $\text{Sb}^{3+}/\text{Sb}^{5+}$  ratio is  $\sim 43/57$ , where  $\text{Sb}^{3+}$  represents around

43% of the ceramic antimony. According to formula (7), and considering that  $Sb(x + x') \cong 0.05$  (Table 1), it is understandable that the carrier concentration reaches  $\sim 1 \times 10^{20} e^- cm^{-3}$ , i.e., close to the above-mentioned value  $1.1 \times 10^{20} e^- cm^{-3}$  deduced from Hall measurement (Table 2). Consequently the enhancement in the conductivity of the  $SnO_2:Sb:Zn$  ceramic is mainly due to the enhancement in the carrier mobility.

#### 4. Conclusions

Co-doping  $SnO_2$  based ceramics with Sb and Zn, showed profound effects on ceramic density, electronic properties and crystal composition. Doping with Sb alone, enhanced the ceramic electrical conductivity, with no densification. On the other hand, Zn-doped ceramics showed enhanced ceramic densification with low conductivity. Ceramics doped with both Sb and Zn ( $SnO_2:Sb:Zn$ ) showed enhanced electrical conductivity and high densities as well. Evidence shows that Zn doping is responsible for retention of Sb in the composition.

#### Acknowledgements

I.S. wishes to thank the French Ministry of Foreign Affairs for providing his scholarship and J.P. Manaud for helpful discussions and advices. H.S.H. is thankful to ARABFUND for a grant.

#### References

- [1] G. McCarthy, J. Welton, *Powder Diffraction* 4 (1989) 156.
- [2] J.P. Coleman, J.J. Freeman, P. Madhukar, J.H. Wagenknecht, *Displays* 20 (1999) 145–154.
- [3] O. Kluth, C. Agash, J. Hüpkens, J. Müller, B. Rech, Magnetron sputtered zinc stannate films for silicon thin film solar cell, in: 3rd World Conference on Photovoltaic Energy Conversion (WCPEC-3), May 11–18, 2003, Osaka, Japan.
- [4] K. Zakrzewska, *Thin Solid Films* 391 (2001) 229–238.
- [5] N.C. Li, C.R. Martin, *J. Electrochem. Soc.* 148 (2001) A164–A170.
- [6] N.L. Wu, J.Y. Hwang, P.Y. Liu, C.Y. Han, S.L. Kuo, K.H. Liao, M.H. Lee, S.Y. Wang, *J. Electrochem. Soc.* 148 (2001) A550–A553.
- [7] D.U. Ju, J.-H. Chung, D.-J. You, S.-G. Kim, *Ind. Eng. Chem. Res.* 37 (1998) 1827–1835.
- [8] S. Shanthi, C. Subramanian, P. Ramasamy, *Mat. Sci. Eng. B* 57 (1999) 127–134.
- [9] E. Shanthi, V. Dutta, A. Banerjee, K.L. Chopra, *J. Appl. Phys.* 5 (1980) 6243–6251.
- [10] K.C. Mishra, K.H. Johnson, P.C. Schmidt, *Phys. Rev. B* 51 (1995) 13972–13976.
- [11] C. Kilic, A. Zunger, *Phys. Rev. Lett.* 88 (2002) 095501.
- [12] S. Shanthi, C. Subramanian, P. Ramasamy, *Cryst. Res. Technol.* 34 (1999) 1037–1046.
- [13] F. Morazzoni, C. Canevali, N. Chiodini, C. Mari, R. Ruffo, R. Scotti, L. Armelao, E. Tondello, L. Depero, E. Bontempi, *Mat. Sci. Eng. C* 15 (2001) 167–169.
- [14] K.S. Kim, S.Y. Yoon, W.J. Lee, K.H. Kim, *Surf. Coat. Technol.* 138 (2001) 229–236.
- [15] J. Zhang, K. Colbow, *J. Appl. Phys.* 71 (1992) 2238–2242.
- [16] A. Messad, J. Bruneaux, H. Cachet, M. Froment, *J. Mater. Sci.* 29 (1994) 5095–5103.
- [17] H. Kima, A. Piqué, *Appl. Phys. Lett.* 84 (2004) 218–220.
- [18] T. Minami, *J. Vac. Sci. Technol. A* 17 (1999) 1765–1772.
- [19] E.R. Leite, J.A. Cerri, E. Longo, J.A. Varela, C.A. Paskocima, *J. Eur. Cer. Soc.* 21 (2001) 669–675.
- [20] E.R. Leite, J.A. Cerri, E. Longo, J.A. Varela, *Cerâmica* 49 (2003) 87–91.
- [21] J.A. Varela, L.A. Perazolli, J.A. Cerri, E.R. Leite, E. Longo, *Cerâmica* 47 (2001) 117–123.
- [22] J. Fayat, M.S. Castro, *J. Eur. Cer. Soc.* 23 (2003) 1585–1591.
- [23] D. Gouvêa, Ph.D. thesis, Limoges University, Limoges, France, 1995.
- [24] O. Scarlat, S. Mihaiu, Gh. Aldica, J. Grozac, M. Zaharescu, *J. Eur. Cer. Soc.* 24 (2004) 1049–1052.
- [25] C. Marcel, Ph.D. thesis, Bordeaux 1 University, Bordeaux, France, 1998.
- [26] S.D. Han, S.Y. Huang, G. Campet, M.A. Kennard, *Act. Pass. Elec. Comp.* 18 (1995) 53–60.
- [27] A. Gamard, O. Babot, B. Jousseume, M.C. Rasclé, T. Toupance, G. Campet, *Chem. Mater.* 12 (2000) 3419–3426.
- [28] R.D. Shannon, *Cryst. Acta A* 32 (1976) 751–767.
- [29] C.G. Fonstad, R.H. Rediker, *J. Appl. Phys.* 42 (1971) 2911–2918.
- [30] L. Petit, K. Richardson, B. Campell, G. Orveillon, T. Cardinal, F. Guillen, C. Labrugere, P. Vinatier, M. Couzi, W. Li, S. Seal, *Phys. Chem. Glasses* 45 (2004) 315–321.
- [31] H.L. Ma, X.T. Hao, J. Ma, Y.G. Yang, J. Huang, D.H. Zhang, X.G. Xu, *Appl. Surf. Sci.* 191 (2002) 313–318.
- [32] B. Thangaraju, *Thin Solid Films* 402 (2002) 71–78.
- [33] E. Elangovan, K. Ramamurthi, *Cryst. Res. Technol.* 38 (2003) 779–784.
- [34] T. Nutz, M. Haase, *J. Phys. Chem. B* 104 (2000) 8430–8437.
- [35] D. Maestre, A. Cremades, J. Piqueras, *Semicond. Sci. Technol.* 19 (2004) 1236–1239.
- [36] *Natl. Bur. Stand. (U.S.) Monogr.* 25 (1972) 62.